Side-chain recognition and gating in the ribosome exit tunnel

Paula M. Petrone*, Christopher D. Snow*, Del Lucent*, and Vijay S. Pande*†‡

*Biophysics Program and †Department of Chemistry, Stanford University, Stanford, CA 94305

Edited by Michael Levitt, Stanford University School of Medicine, Stanford, CA, and approved August 29, 2008 (received for review February 25, 2008)

The ribosome is a large complex catalyst responsible for the synthesis of new proteins, an essential function for life. New proteins emerge from the ribosome through an exit tunnel as nascent polypeptide chains. Recent findings indicate that tunnel interactions with the nascent polypeptide chain might be relevant for the regulation of translation. However, the specific ribosomal structural features that mediate this process are unknown. Performing molecular dynamics simulations, we are studying the interactions between components of the ribosome exit tunnel and different chemical probes (specifically different amino acid side chains or monovalent inorganic ions). Our free-energy maps describe the physicochemical environment of the tunnel, revealing binding crevices and free-energy barriers for single amino acids and ions. Our simulations indicate that transport out of the tunnel could be different for diverse amino acid species. In addition, our results predict a notable protein–RNA interaction between a flexible 23S rRNA tetraloop (gate) and ribosomal protein L39 (latch) that could potentially obstruct the tunnel's exit. By relating our simulation data to earlier biochemical studies, we propose that ribosomal features at the exit of the tunnel can play a role in the regulation of nascent chain exit and ion flux. Moreover, our free-energy maps may provide a context for interpreting sequence-dependent nascent chain phenomenology.

fragment-based search | free-energy calculation | molecular dynamics | simulation | translation

In recent years, experimental evidence has accumulated revealing that the ribosomal tunnel could play an important role in cotranslational regulation of protein secretion (refs. 1–9, among other relevant studies). For example, the secM peptide binds to the narrowest constriction of the tunnel, between ribosomal proteins L4 and L22, which protrude into the tunnel, causing translation arrest, which is required *in vivo* to elevate the frequency of secA translation (2). Sequence-dependent translation arrests, such as the case of the secM peptide, have led scientists to propose that the ribosomal tunnel could act as a discriminatory "gate" for proteins [Nakatogawa and Ito (1) and other works reviewed in ref. 4)]. The involvement of particular L22 residues and specific domains of 23S rRNA suggest that there is some kind of signal-transmission mechanism (1) from the tunnel components to the peptidyl transferase center (PTC). In addition, studies show that some regulatory peptides like secM (3) or tnaC (6, 7) require the presence of a nonpolypeptide cofactor for stalling. Other examples of intraribosomal signal transmission have been identified. For example, macrolide antibiotics (10) appear to disable ribosomal function by obstructing the exit tunnel at the constriction site or by triggering a conformational change in L22 that propagates along the tunnel (11, 12). Liao *et al.* (13) found that the ribosome tunnel is responsible for recognizing nascent membrane proteins and recruiting translocon assistance, based on interactions between the nascent chain and an alleged tunnel sensor, protein L39. However, it is not yet known how the signal is transmitted from L39 to the translocon-binding regions at the tunnel's surface. The studies by Dresios *et al.* (5), show that the absence of ribosomal protein L39—a small protein located near the exit of the tunnel—increases the rate of binding of aminoacyl-tRNA to the A-site and diminishes the accuracy of translation.

Overall, these findings depict the ribosomal tunnel as a protein-sensitive channel with an active role in sequence recognition and regulation of translation. Important questions follow from these studies: What is the nature of the chemical environment inside the tunnel such that it allows sequence-specific regulation of translation? Which are the specific ribosomal features that give rise to such an environment?

X-ray structures let us appreciate—at atomic resolution—the complex architecture of the ribosome [for example, Schuwirtz *et al.* (14) and Ban *et al.* (15)]. Computer simulations allow researchers to set these static structures in motion and explore otherwise-inaccessible temporal and spatial regimes, yielding characterizations of global ribosomal electrostatics (16) and large-scale motions (17, 18).

Unlike earlier modeling efforts (16–18), we focus on the ribosome tunnel to elucidate its role in the regulation of translation. Our computational approach combines calculation of free energies and a fragment-based scan of the molecular surface of the ribosome tunnel. The function of a biomolecule is associated with its ability to interact with ligands. In the case of the ribosome tunnel, the ligand is the nascent polypeptide that interacts with the structural proteins and nucleotides that comprise the ribosome tunnel. We scan the inner surface of the tunnel with fragments of the nascent polypeptide. Our set of probes consists of various single amino acid side chains that represent various chemical functionalities present in the nascent chain (hydrophobic, charged, large, small, and aromatic). In a similar fashion, we probe the tunnel with Cl^- and Na^+ ions to assess their accessibility in the tunnel. By our method, however, the simulated chemical probes are separated in space to prevent their mutual interactions. Technical details of our methods can be found in *Methods*. We perform thermodynamic sampling on an unprecedented scale ($\approx$10 ns per Å^3), calculating comprehensive maps of the 3D potential of mean force (PMF) for single amino acid analogs and ions throughout the ribosomal exit tunnel. These maps directly illustrate binding sites and energetic barriers that may approximate the interactions recognized by the side chains in the nascent polypeptide, suggesting sequence-dependent pathways of amino acid side chains in their way out of the ribosome. We verified differences in accessibility between Na^+ and Cl^- ions at the exit of the tunnel. Furthermore, our simulations reveal an arginine-mediated RNA–protein interaction between ribosomal components, acting as a ribosomal valve, whose rapid fluctuations (approximate nanosecond time scale)

Author contributions: P.M.P., C.D.S., and V.S.P. designed research; P.M.P. and V.S.P. performed research; P.M.P. and D.L. contributed new reagents/analytic tools; P.M.P. analyzed data; and P.M.P. and V.S.P. wrote the paper.

The authors declare no conflict of interest.

This article is a PNAS Direct Submission.

‡To whom correspondence should be addressed at: Clark Center S294, 318 Campus Drive, Stanford, CA 94305-5080. E-mail: pande@stanford.edu.

This article contains supporting information online at www.pnas.org/cgi/content/full/0801795105/DCSupplemental.

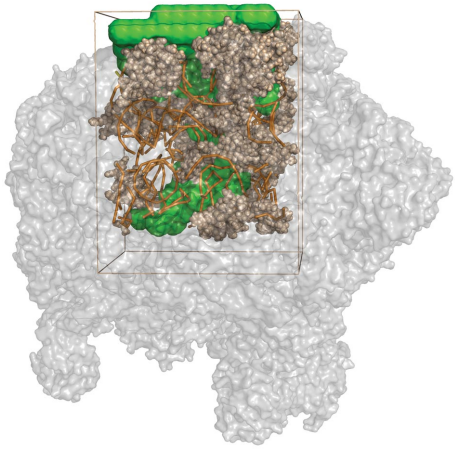

Fig. 1. Large-subunit *Haloarcula marismortui* (PDB ID code 1S72) and in-box simulated model. Tan, modeled rRNA (tubes) and protein (spheres); green, solvent-accessible volume.

occlude the tunnel's exit and could potentially affect the rate of peptide translocation or ion flux.

Results

Free-Energy Landscape of the Exit Tunnel Is Amino Acid-Dependent. Using an all-atom model of a fragment of the *Haloarcula marismortui* ribosome including the exit tunnel (see Fig. 1 and *Methods*), we calculated a PMF for tryptophan, alanine, isoleucine, lysine, and aspartate to probe the reactivity of the environment to aromatic, small, hydrophobic and charged species. This calculation yields positional free-energy profiles for each side-chain analog in the entire solvent-accessible volume inside the ribosome tunnel (Fig. 2). At first sight, the profiles in Fig. 2 show that the tunnel's molecular surface, far from being energetically smooth, presents an intricate landscape with free-energy barriers and local free-energy minima. Moreover, free-energy profiles notably vary between different amino acid species, indicating that, considering solely the effect of the isolated side chains, transport of these amino acids through the tunnel could be inherently different.

Despite noticeable physicochemical differences, all of the profiles share an unexpected feature in common: Large free-energy barriers lie at the tunnel's exit, where the amino acid probes would be expected to experience higher entropic freedom and fewer interactions with the ribosome. Fig. 3 shows a 1D projection of the binding free energy along the longitudinal axis of the ribosome tunnel. On the main axis of the tunnel, there is a significant free-energy barrier for lysine ($\approx 7\ k_BT$), isoleucine ($\approx 5\ k_BT$), and tryptophan ($\approx 6\ k_BT$) at the exit. On the other hand, for aspartate ($\approx 2\ k_BT$) and alanine ($\approx 1\ k_BT$), this barrier is smaller. These results indicate that the free-energy barrier at the exit of the tunnel depends on the chemical group, being significantly lower for small and negatively charged amino acids like alanine and aspartate, respectively. Relating this data to the free-energy maps of charged ions, we can observe that this free-energy barrier depends not only on the size and composition but also on the charge of the chemical probes.

Fig. 4, supporting information (SI) *Text*, and Figs. S1 and S2 show the free-energy profiles for Cl^- and Na^+ ions in the tunnel, illustrating the affinity and accessibilities of these chemical species. These profiles were calculated by following the same protocol as with the charged amino acid free-energy maps. Our calculations show that the walls of the tunnel are unfavorable to Cl^- ions. Accessibility of Cl^- increases away from the walls, as noticed in the spacious section between the PTC site and the constriction site. The constriction site seems particularly accessible to Cl^-. Positive residues from both L22 and L4 protrude into the tunnel at this narrow point as shown in Fig. S1*C*. Accessibility of Cl^- decreases toward the exit of the tunnel ($1 < \Delta G < 5\ k_BT$) nearby a 23S rRNA tetraloop (residues 494–497) and arginines in L39. On the other hand, there is high affinity ($\Delta G < -5\ k_BT$) for Na^+ ions throughout the tunnel (Fig. S2*C*), especially lining the walls. In particular, near the exit, the accessibility of Na^+ is high. Areas for reduced accessibility for Na^+ ($\Delta G > 7\ k_BT$) are shown in Fig. S2*D* and include the regions nearby the PTC site, the constriction site, and arginines in L39.

Characterizing a Rapidly Fluctuating RNA–Protein Interaction. Amino acid and Cl^- maps see free-energy exclusion at the exit of the

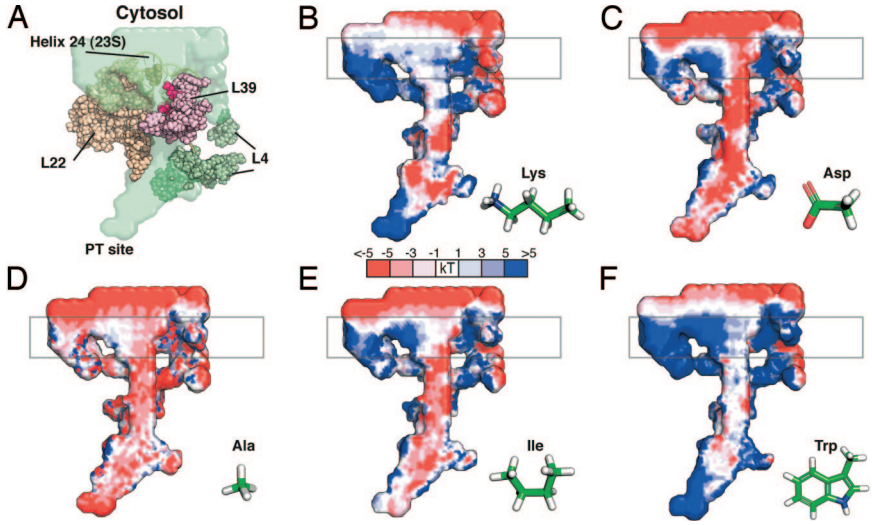

Fig. 2. Free-energy maps of the chemical environment inside the ribosome tunnel simulated with molecular dynamics. (*A*) Inner-tunnel volume (green) and proteins near the ribosome tunnel. The gate A497 in helix 24 is highlighted in spheres. In dark-pink spheres, arginines of L39. (*B–F*) Free-energy profiles for single amino acid side chains in the tunnel. Each graph is a transverse cut of the tunnel; the exit to cytosol is at the top and peptidyl transferase center at the bottom. Free energies are measured in k_BT with reference to each probe's solvated state outside the tunnel. Red-colored areas are regions of favorable residence; white denotes neutral areas. High free-energy areas are represented in increasing tones of blue (error analysis is in Fig. S13). Boxed in gray, location of free-energy barrier predicted by our simulations.

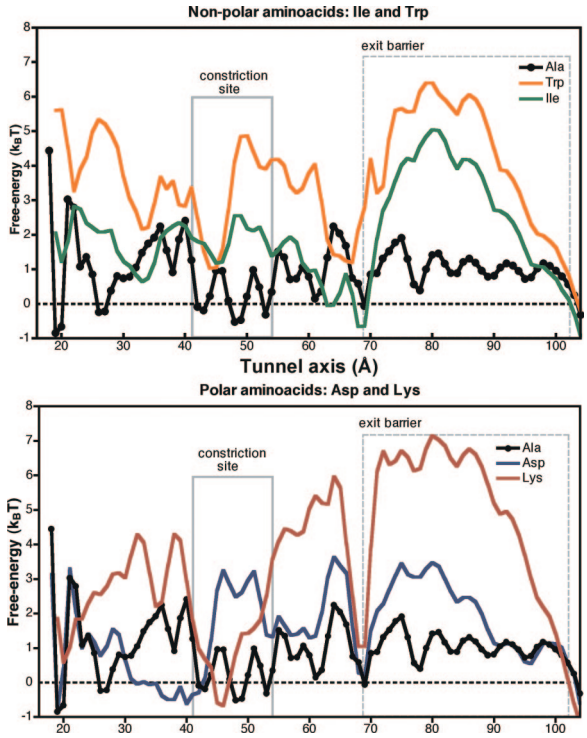

Fig. 3. Free-energy profiles along the longitudinal axis of the ribosomal tunnel. The scale corresponds to the structural elements as shown in Fig. S14. Flexible parts of simulated model located in the range 20–105 Å. (*Upper*) Hydrophilic side chains Asp and Lys. (*Lower*) Hydrophobic side chains Trp and Ile. Boxed in dashes, free-energy barrier predicted by our simulations. The uncertainty to the free-energy profiles is plotted in Fig. S15.

tunnel. This free-energy barrier seems reduced for the small probes alanine and aspartate, and there is no free-energy barrier for Na^+ ions. What is the structural cause of this differential free-energy barrier? Flexible structural components near the exit of the tunnel were identified by analyzing control trajectories of a simulated model that includes only the ribosome tunnel, water, and ions and no amino acid probes (*Methods* in *SI Text*). The root mean square displacements (RMSD) of the atoms at the end of the tunnel revealed a striking feature of the tunnel's dynamical activity: a very flexible rRNA segment (hereafter referred to as the gate) and nearby positively charged residues from protein L39 (hereafter, referred to as the latch) (see Movie S1 and Movie S2). The large RMSD fluctuations from our simulations correspond well with the crystallographic B factors, which show peaks of B >80 Å (2) both for atoms of the gate and latch L39 (see *Discussion* in *SI Text* and Fig. S3). The histogram of distances (Fig. 4*B*) show that the distance between A497 and the group of arginines (R20, R31, and R39) of L39 can deviate ≈8 Å from the crystal structure value of 9.5 Å and exhibits additional peaks at 2.8 Å and 4.8 Å, suitable distances for hydrogen bonds and water-mediated hydrogen-bond interactions, respectively.

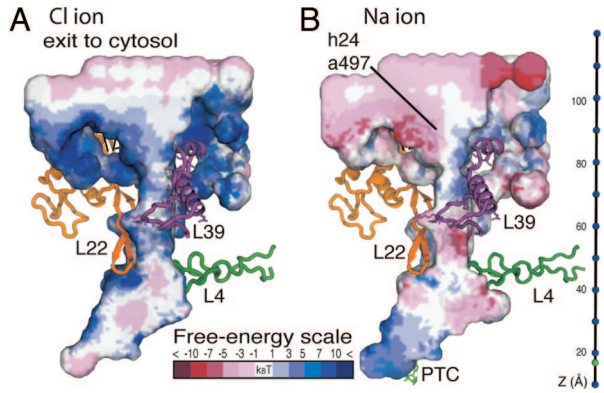

Fig. 4. Transversal cut of the free-energy profile for Cl^- and Na^+ ions in the ribosome exit tunnel. Free energies are measured in k_BT with reference to each ion's solvated state outside the tunnel.

Discussion

The Tunnel as a Protein-Sensitive Channel. Each of the free-energy calculation profiles in Fig. 2 is markedly different, indicating that the molecular surface interior to the tunnel is indeed sensitive to the variation in chemical species, in agreement with the results of recent experiments (2, 8, 9, 13, 19, 20).

Alanine is a small molecule with no functional groups and, for a nonpolar molecule, little hydrophobicity. The tunnel's environment for alanine does not seem much different from that of bulk solvent. This is also reflected by the sharp peak near solvation free energy in the free-energy histogram (see *Discussion* in *SI Text* and Fig. S4).

The tunnel presents an inhospitable environment for the hydrophobic probes tryptophan and isoleucine (Fig. 2 *E* and *F*). The free energy profiles reflect overall unfavorable free energy, even along the most spacious central axis of the tunnel. In the tunnel, water is a preferred occupant over hydrophobic side chains, thus reducing significantly their accessible volume in the tunnel. This is especially true for tryptophan at the constriction site.

Reports indicate that the constriction site is an essential feature for ribosome stalling mediated by a specific nascent sequence, such as in secM (2). Tryptophan, present in a similar position in both the tnaC and secM peptides, is thought to be important for ribosome stalling (6, 7). In addition, some specific mutations of key residues at the constriction relieve stalling (1, 6, 7), although other additional features of these stalling sequences like compaction (8) or binding of cofactors (3, 6) also seem to be crucial for stalling. Consistent with these reports, Fig. 2*F* and Fig. S5 show that tryptophan has a sizable free-energy barrier at the tunnel constriction ($\Delta G > 4k_BT$).

For the hydrophilic species, the tunnel creates a rugged free-energy landscape. As seen in Fig. 2 *B* and *C*, lysine and aspartate acid have inverted free-energy profiles: Where lysine has energy barriers, aspartate has energy depressions and vice versa. Because the constriction site is hydrophilic, the charged probes do not suffer significant energy barriers at this relatively narrow location. Aspartate has a favorable pocket near positive residues of L22. In addition, whereas lysine exhibits a large free-energy barrier at the exit of the tunnel, aspartate seems to find easier access to this region (Fig. 2*C*).

Lu *et al.* (9) have experimentally measured accessibilities of amino acids based on the relative ratios of modification rate constants for specific nascent chain side chains at discrete positions in the tunnel using a cysteine-substituted molecular tape measure derived from the Kv1.3 protein. This interesting study proposes that the electrostatic potentials in the tunnel are dynamic and regulated by the presence of the nascent chain. By a thorough scan of the tunnel, our computational approach also captures the fact that the different accessibilities for single chemical probes depend not only on charge but also on the size of the probes as suggested by Lu *et al.* Our study includes both the enthalpic and the entropic contributions from the interactions. In addition, our maps highlight features of the tunnel with potential functional roles.

The free-energy maps of the various probes characterize the chemical environment of the tunnel. These maps could be

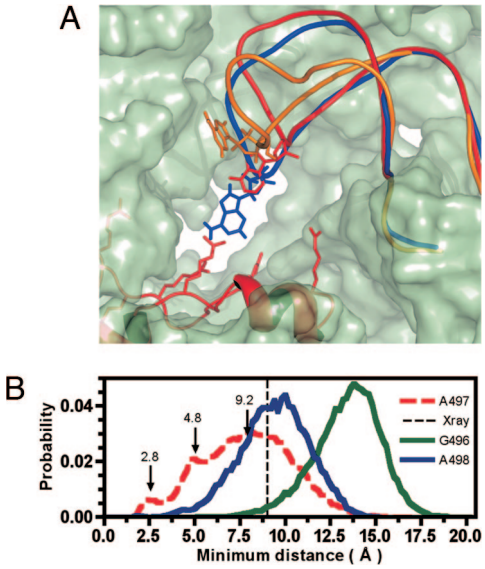

Fig. 5. Conformational change of the tip of rRNA helix24 (gate) relative to arginines in L39 (latch) predicted with MD simulations. (*A*) Exterior view of the ribosome tunnel. Shown are A497 in sticks and x-ray structure in red. In blue, A497 is 2.7 Å away from the closest arginine. In orange, A497 is 16.7 Å away from the closest arginine. (*B*) Histogram of minimum distance between the rRNA tetraloop and L39. Each curve shows the interactions of rRNA bases G496, A497 and A498, with arginines (R20, R31, and R39) in L39. Two close-contact peaks are shown at 2.8 Å and 4.8 Å for A497 and the maximum at 7.8 Å. In dashes, the x-ray minimum distance of 9.04 Å (details in *SI Text Discussion*).

extrapolated to understand the interactions between the nascent chain and the tunnel. However, caveats of this extrapolation include a probable overestimation of the molecular surface of the tunnel accessible to amino acid side chains as compared with the accessibility of the nascent chain. As part of the nascent chain, the peptide bond between any pair of consecutive residues restricts the mobility of side chains in the tunnel. These restraints might be particularly relevant at the narrower points in the tunnel, such as the constriction site, increasing the size of the free-energy barriers compared with those barriers suffered by the individual side chains in those regions. The added value of this PMF data resides in its use as force field for molecular dynamics (MD) simulations of the nascent chain in the tunnel with the proper backbone restraints.

The free-energy maps of Cl^- and Na^+ probes show the affinity of these ions for the tunnel. The negative Cl^- probe shows low affinity for the walls of the rRNA-lined tunnel (Fig. S1*C*), especially at the exit where the accessibility of Cl^- is reduced. On the other hand, Na^+ ions find many favorable regions in the tunnel, especially between the constriction site and PTC (Fig. S2*C*). At the constriction site, there is a region of low accessibility for Na^+ ions near positive residues in the loops of L4 and L22 protruding into the tunnel.

A MD fragment-based scan of the molecular surface reveals dynamic features of the surface. For example, the free-energy maps of ions and single amino acids point out to a very singular protein–RNA interface: a very flexible RNA loop interacting with arginines in ribosomal L39. Its relative displacement becomes evident in the trajectory as a gate held closed by a latch.

Gate–Latch Hypothesis for Peptide-Free Ribosomes. We identify the tetraloop (residues 494–497) at the tip of helix 24 in the 23S as the ribosome gate. In our probe-free simulations, we found that A497 interacts with the highly-positive electrostatic potential provided by L39 (the latch). The latch L39 is located opposite to the gate with respect to the tunnel's opening (Fig. 5). Our simulations predict that, in a peptide-free ribosome, the gate obstructs the tunnel by approaching the latch and making short-range interactions with the latch's positive residues.

In the original x-ray structure of the ribosome [PDB ID code 1S72 (15)] (Fig. 5), the gate A497 was crystallized at the exit of the tunnel. Most of the time, the gate dwells in a "capping state," blocking the entrance. However, we find rare events in which most of helix 24 sways away from the tunnel's entrance for a few picoseconds, leaving the exit clear, and promptly returns to its capping state as a valve that is closed but momentarily opens. The broad conformational change of the tip of helix 24 is shown in Fig. 5. In addition, Fig. S6 shows a contour map representing the probability of finding A497 at the tunnel's exit. This region fluctuates rapidly, making it possible to capture complete transitions with short (20-ns) trajectories (Movie S1 and Movie S2), given a sufficient number of simulations to observe this event.

Regarding the latch, one should also consider the nature of L39, a 50-residue protein that contains several arginines. Arginine contains three terminal groups (two amino and one amide) that can donate hydrogen bonds to appropriate acceptor groups and allow an extensive network of contacts (21). Because of this, arginine is very effective at forming RNA–protein interfaces (21, 22).

Specifically in the ribosome tunnel, the x-ray structure (PDB ID code 1S72) shows that nearby A497 (within 10 Å) are L39's arginine side chains (R20, R31, and R35), and the four more distant (14–25 Å) arginine side chains (R39, R40, R43, and R44) are directed into the tunnel cavity. Our simulations indicate that A497 maintains short-range interactions with R20 and R31 (2.8 and 4.8 Å, respectively) and suggest longer-range interactions (<10 Å) with R35 and R39 (see *Discussion* in *SI Text*).

Simulations in our work were performed on the *Haloarcula marismortui* ribosome. Free-energy calculations were extremely computationally costly (equivalent to ≈388 years on a single processor). Given the cost of reproducing the calculation in other ribosomes, it is pertinent to combine our data with conservation arguments and speculate about the validity of these predictions in other organisms. In this spirit, we verify the sequence and structural conservation of the agents that constitute the electrostatic interface at the exit of the tunnel: ribosomal protein L39 and the tip of rRNA helix 24. We would expect that both agents (or suitable replacements) should be present in other ribosomes exhibiting similar electrostatic charge as well as dimensions as a necessary requirement for this model. Fig. 6 shows a local alignment of the *H. marismortui* structure (PDB ID code 1s72) used in our simulation to published x-ray structures of ribosomes: *E. coli* [PDB ID code 2AW4 (14)], *Deinococcus radiodurans* [PDB ID code 1NKW (23)], and *Thermus thermophilus* [PDB ID code 1VSA (24)]. Details on the sequence and structural alignment are provided in *Discussion* in *SI Text*.

To begin with, the importance of L39 is suggested by its conservation in archea and mammals (25). The basic motif KRRHWRRTKL in L39 that includes R39, R40, R43, and R44 is highly conserved among the different species. Tsui *et al.* (25) also report conservation of R20 and R35. In eubacteria, L39 is not present, but it has previously been suggested (23) that it is replaced by the tail of L23. Fig. 6 shows that a region of L23 in *D. radiodurans* not only superposes well with L39 of *Haloarcula*, but also includes R62, R64, and R67 among four other nearby positively charged residues. In the case of *T. thermophilus*, Fig. 6 also shows a similar structural superposition for the tip of L23 and L39, with R65 and R68 among several positively charged residues. Similarly, Fig. 6 shows that in the tail of L23 of *E. coli* —exposed to the tunnel—there is a stretch of nine residues (69–77), four of which are arginines. Additionally, these arginines show large B factors [$B > 89$ Å^2] in the crystal structure of *E. coli* [PDB ID code 2AW4 (14)] that could result from structural fluctuations.

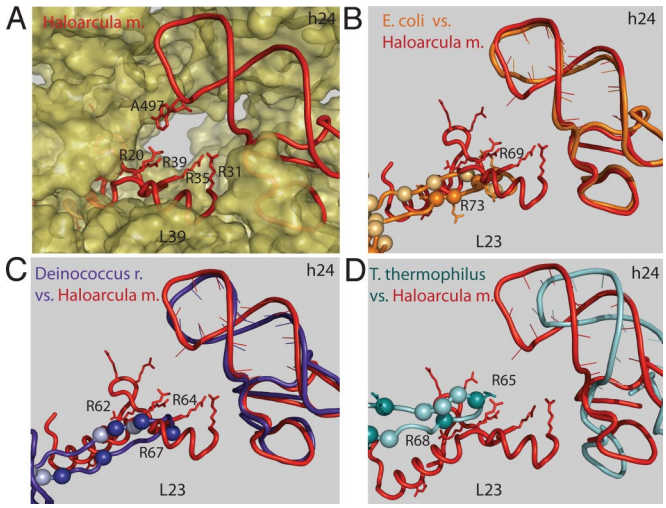

Fig. 6. Structural alignment of different ribosome x-ray structures to *H. marismortui* (in red color, PDB ID code 1S72). Exterior view of the exit of the ribosomal tunnel that shows rRNA helix 24 from 23S and proteins L23 and L39. Positive residues are in spheres, and arginines are in dark spheres and sticks. (*A*) *H. marismortui* [PDB ID code 1S72 (15)]. (*B*) *E. coli* [PDB ID code 2AW4 (14)], in orange. (*C*) *D. radiodurans* [PDB ID code 1NKW (23)], in blue. (*D*) *T. thermophilus* [PDB ID code 1VSA (24)], in cyan.

With regard to the tip of rRNA helix 24, the corresponding regions in both *E. coli* and *Deinococcus* consistently resemble the *Haloarcula* structure. The same observation holds for *T. thermophilus*, although in this case, this region seems slightly displaced. The main difference between different organisms resides in the fact that *E. coli* has an insertion that makes this region a pentaloop instead of a tetraloop as in *Haloarcula* (Sequence alignment and secondary structure prediction in *Discussion* in *SI Text*). In *Haloarcula*, the flexibility of this tail viewed in our simulation allows this tetraloop to contact arginines in L39. In the case of a pentaloop, an additional base in the rRNA loop might allow greater degrees of freedom for movement and additional polar contacts. Looking at the predictions for other species, we found that the tip of this helix can adopt either a tetraloop or pentaloop, or even a hexaloop as in *Homo sapiens* (Fig. S7).

Connections to Previous Experiments. How does the gate–latch hypothesis relate to the free-energy barrier for single amino acid and ion probes at the exit of the tunnel? In the case of a peptide-free ribosome, it is possible that the gate–latch interface causes an exclusion for Cl^- ions that is captured in the reduced accessibility of Cl^- probes at the exit of the tunnel (Fig. 4*A*). The issue of ion permeability through the ribosome–translocon pore has been addressed before. Johnson *et al.* (13, 26) have observed that fluorophores inside the ribosome–translocon pore cannot be quenched by iodide ions added to the cytosol. Our prediction of an obstruction of the tunnel cross-section by a flexible rRNA loop that opens and closes is not inconsistent with those experiments.

In the case of the amino acid probes, our simple gate–latch model for a peptide-free ribosome becomes a multibody problem. The arginines in L39, the flexible rRNA, the single-molecule probe and the solvent all become part of an interplay of competing energetics. In our simulation, all of the amino acid probes except for Asp and Ala, find unfavorable interactions at the exit of tunnel, although it is not clear whether it is due to a probe–rRNA, probe–arginine, or rRNA–arginine interaction or a combination of all three possibilities, mediated by solvent. Extrapolating to the nascent polypeptide, it is difficult to assess how the gate will interact with the elongating peptide. Plausible scenarios in which the gate is constantly open involve interactions between chaperones and the gate helix 24, or the nascent chain itself blocking the gate–latch interface. A "hose-clamp" scenario involves the tip of helix rRNA interacting with L39 and the peptide, with an effect on the rate of translation.

Regulatory roles of L39 are consistent with our model of a free-energy barrier at the exit of the tunnel and have been previously established. Dresios *et al.* (5) demonstrated that the absence of L39 allows ribosomes to translate faster but with a fourfold increase in error frequency. Because L39 is a small protein in the large subunit, distant from the tRNA-binding A-site in the small subunit, it is natural to ask how the effect of L39's absence can be communicated to the peptidyl transferase center in the large subunit and the A-site in the small subunit to disrupt the normal translation rate and accuracy, respectively.

We propose that this propagation occurs by interaction between L39 and the A-site: via the nascent chain. If the absence of L39 makes translation faster but less accurate (5), it is natural to hypothesize that L39 contributes to an energetic barrier to the nascent chain that could serve to ensure a safe rate of translation, as well as to protect the tunnel exit from unwanted guests. In our model, this barrier consists of a multibody interaction between the nascent chain, positively charged residues of L39—highly exposed in the tunnel's volume—and the tip of helix 24, a flexible rRNA tetraloop at the tunnel's exit. Even though the x-ray structure (PDB ID code 1S72) shows that L39 is far (≈9.5 Å) from helix 24, our simulation predicts that these two elements can get as close as 2.4 Å from each other because of the flexibility of the rRNA region and the interaction with positive residues that are strategically located in L39. Helix 24 has been reported to contact the protein conducting channel (PCC) (27, 28), and the flexibility of this loop might also serve for that role.

In conclusion, the energy landscape presented in this work, and its impact, will likely be modified by the presence of all active participants in the ribosome–translocon–peptide complex, including the nascent peptide and chaperones. Nevertheless, our findings may provide critical insights into the environment of the tunnel and its role in translation.

Methods

As a starting point for MD simulation, we used a cut-out of ≈80,000 atoms cropped out from *H. marismortui* large subunit (PDB ID code 1S72) (15) (see *Methods* in *SI Text* for assumptions of the model). We capped protein and RNA at the cut-out boundaries. The dimensions of the model are $82.5 \times 85 \times 110$ Å^3 in agreement with previous geometric and functional analysis of the length the tunnel (29, 30), and it encompasses the ribosomal exit tunnel and its surrounding areas (Fig. 1) as well as a buffer of exterior water. All atoms at a distance of 10 Å from the tunnel inner available volume were held fixed. Parameters were taken from the AMBER parameter dataset (http://pharmacy.man.ac.uk/amber/). Initial coordinates for crystallographic water and ions were retained, and excess negative charge was balanced with sodium atoms. Single amino acid and ion probes were placed on a grid that covered the entire available volume inside the tunnel. Multiple runs ensured that probes proximal in the grid would not interact with each other. Runs were parallelized in the Folding@Home distributed computing network. Details of modeling and simulation are available in *Methods* in *SI Text*. Probe positional data were analyzed by using WHAM (31, 32) umbrella-sampling algorithm extended to three dimensions, yielding PMF maps of the center of mass of single amino acids in the ribosome tunnel. One can find further details on the free energy calculation in *Data and Error Analysis* in *SI Text*. Additional Figs. S8–S12 and Tables S1 and S2 are available for this article.

ACKNOWLEDGMENTS. We thank the Folding@Home community for the computer power; J. Dresios, D. Hershlag, C. Yanofsky, R Cruz Vera, J. Puglisi, H. Herce, E. Goldini, J. Chodera, S. Park, D. Ensign, V. Voeltz, Madhusudhan, M. Topf, M. Raschi, and the V.S.P. laboratory for valuable discussion; the anonymous reviewers for their insightful comments and improvements to the original manuscript; L. Forbes for editing; family and friends for encouragement; and Instituto Balseiro, Argentina. Molecular images were drawn with Pymol. Movies were rendered with VMD. This work was supported by the National Institutes of Health (NIH) and the National Science Foundation (NSF), in particular Simbios (NIH U54 GM072970) and NSF Frontiers in Integrative Biological Research (NSF EF-0623664).

1. Nakatogawa H, Ito K (2002) The ribosomal exit tunnel functions as a discriminating gate. *Cell* 108:629–636.
2. Nakatogawa H, Ito K (2004) Intraribosomal regulation of expression and fate of proteins. *ChemBioChem* 5:48–51.
3. Muto H, Nakatogawa H, Ito K (2006) Genetically encoded but nonpolypeptide prolyl-tRNA functions in the A site for SecM-mediated ribosomal stall. *Mol Cell* 22:545–552.
4. Mankin AS (2006) Nascent peptide in the ''birth canal'' of the ribosome. *Trends Biochem Sci* 31:11–13.
5. Dresios J, Derkatch IL, Liebman SW, Synetos D (2000) Yeast ribosomal protein L24 affects the kinetics of protein synthesis and ribosomal protein L39 improves translational accuracy, while mutants lacking both remain viable. *Biochemistry* 39:7236–7244.
6. Gong F, Ito K, Nakamura Y, Yanofsky C (2001) The mechanism of tryptophan induction of tryptophanase operon expression: Tryptophan inhibits release factor-mediated cleavage of TnaC-peptidyl-tRNA(Pro). *Proc Natl Acad Sci USA* 98:8997–9001.
7. Cruz-Vera LR, Rajagopal S, Squires C, Yanofsky C (2005) Features of ribosome–peptidyl–tRNA interactions essential for tryptophan induction of tna operon expression. *Mol Cell* 19:333–343.
8. Woolhead CA, Johnson AE, Bernstein HD (2006) Translation arrest requires two-way communication between a nascent polypeptide and the ribosome. *Mol Cell* 22:587–598.
9. Lu J, Kobertz WR, Deutsch C (2007) Mapping the electrostatic potential within the ribosomal exit tunnel. *J Mol Biol* 371:1378–1391.
10. Yonath A (2005) Antibiotics targeting ribosomes: Resistance, selectivity, synergism and cellular regulation. *Annu Rev Biochem* 74:649–679.
11. Berisio R, *et al.* (2003) Structural insight into the role of the ribosomal tunnel in cellular regulation. *Nat Struct Biol* 10:366–370.
12. Gabashvili IS, *et al.* (2001) The polypeptide tunnel system in the ribosome and its gating in erythromycin resistance mutants of L4 and L22. *Mol Cell* 8:181–188.
13. Liao S, Lin J, Do H, Johnson AE (1997) Both lumenal and cytosolic gating of the aqueous ER translocon pore are regulated from inside the ribosome during membrane protein integration. *Cell* 90:31–41.
14. Schuwirth BS, *et al.* (2005) Structures of the bacterial ribosome at 3.5 A resolution. *Science* 310:827–834.
15. Ban N, Nissen P, Hansen J, Moore PB, Steitz TA (2000) The complete atomic structure of the large ribosomal subunit at 2.4 A resolution. *Science* 289:905–920.
16. Baker NA, Sept D, Joseph S, Holst MJ, McCammon JA (2001) Electrostatics of nanosystems: Application to microtubules and the ribosome. *Proc Natl Acad Sci USA* 98:10037–10041.
17. Tama F, Valle M, Frank J, Brooks CL, III (2003) Dynamic reorganization of the functionally active ribosome explored by normal mode analysis and cryo-electron microscopy. *Proc Natl Acad Sci USA* 100:9319–9323.
18. Sanbonmatsu KY, Joseph S, Tung CS (2005) Simulating movement of tRNA into the ribosome during decoding. *Proc Natl Acad Sci USA* 102:15854–15859.
19. Tenson T, Ehrenberg M (2002) Regulatory nascent peptides in the ribosomal tunnel. *Cell* 108:591–594.
20. Woolhead CA, McCormick PJ, Johnson AE (2004) Nascent membrane and secretory proteins differ in FRET-detected folding far inside the ribosome and in their exposure to ribosomal proteins. *Cell* 116:725–736.
21. Calnan BJ, Tidor B, Biancalana S, Hudson D, Frankel AD (1991) Arginine-mediated RNA recognition: The arginine fork. *Science* 252:1167–1171.
22. Blachnio K, Przykorska A (2005) Specific arginine mediated RNA recognition. *Postepy Biochem* 51:339–344.
23. Harms J, *et al.* (2001) High resolution structure of the large ribosomal subunit from a mesophilic eubacterium. *Cell* 107:679–688.
24. Korostelev A, Trakhanov S, Laurberg M, Noller HF (2006) Crystal structure of a 70S ribosome-tRNA complex reveals functional interactions and rearrangements. *Cell* 126:1065–1077.
25. Tsui SK, Lee SM, Fung KP, Waye MM, Lee CY (1996) Primary structures and sequence analysis of human ribosomal proteins L39 and S27. *Biochem Mol Biol Int* 40:611–616.
26. Crowley KS, Liao S, Worrell VE, Reinhart GD, Johnson AE (1994) Secretory proteins move through the endoplasmic reticulum membrane via an aqueous, gated pore. *Cell* 78:461–471.
27. Mitra K, *et al.* (2005) Structure of the *E. coli* protein conducting channel bound to a translating ribosome. *Nature* 438:318–324.
28. Halic M, *et al.* (2006) Following the signal sequence from ribosomal tunnel exit to signal recognition particle. *Nature* 444:507–511.
29. Lu J, Deutsch C (2005) Folding zones inside the ribosomal exit tunnel. *Nat Struct Mol Biol* 12:1123–1129.
30. Voss NR, Gerstein M, Steitz TA, Moore PB (2006) The geometry of the ribosomal polypeptide exit tunnel. *J Mol Biol* 360:893–906.
31. Kumar S, Bouzida D, Swendsen R, Kollman P, Rosenberg J (1992) The weighted histogram analysis method for free-energy calculations on biomolecules. I. The method. *J Comput Chem* 13:1011–1021.
32. Bartel C, Karplus M (1887) Multidimensional adaptive umbrella sampling: Applications to main chain and side chain peptide conformations. *J Comput Chem* 18:1450–1462.
Vol. 105, No. 699